Energy Storage Materials 22 (2019) 256–264

Contents lists available at ScienceDirect

Energy Storage Materials

journal homepage: www.elsevier.com/locate/ensm

A new high ionic conductive gel polymer electrolyte enables highly stable quasi-solid-state lithium sulfur battery

Jinqiu Zhou[1], Haoqing Ji[1], Jie Liu, Tao Qian*, Chenglin Yan*

Soochow Institute for Energy and Materials Innovations, College of Energy, Key Laboratory of Advanced Carbon Materials and Wearable Energy Technologies of Jiangsu Province, Soochow University, Suzhou 215006, China

ARTICLE INFO

Keywords:
Gel polymer electrolyte
Quasi-solid-state
Lithium sulfur battery
High ionic conductivity

ABSTRACT

Solid-state lithium battery is regarded as high safety and high energy density next-generation energy storage device, but its poor lithium ionic conductivity severely limits its practical application. To address above issues, we report a new super-high ionic conductive gel polymer (SHGP) electrolyte (2.2×10^{-3} S cm^{-1} at 60 °C and 0.75×10^{-3} S cm^{-1} at 30 °C), which are significant characteristics for greatly improved quasi-solid-state lithium sulfur battery performance. Moreover, the SHGP electrolyte exhibited strong adsorptivity to lithium polysulfides as the polar functional groups in the SHGP electrolyte through chemical adsorption, leading to the suppressed shuttle effect, which was theoretically confirmed by density functional theory (DFT) calculations, molecular dynamics (MD) simulations and experimentally verified by *in-situ* UV/Vis results. Such high ionic polymer electrolyte enables a greatly improved specific capacity of 950 mAh g^{-1} at 0.2 C and outstanding cycling performance for 400 cycles at 1.5 C, which is far beyond that of conventional poly (ethylene oxide) based quasi-solid-state battery.

1. Introduction

Solid-state lithium battery is regarded as one of the next-generation energy storage devices because of its high safety, high energy density and excellent stability [1,2]. The electrolyte, as a crucial part of solid-state battery, provides lithium ions, a pathway for ion transport, and insulation to prevent electron transfer between cathode and anode [3,4]. Liquid organic electrolyte has been widely used for lithium ion batteries (LIBs). However, LIBs operating on liquid organic electrolyte face a severe safety concern such as material defects, electrolyte leakage, and combustion due to the intrinsic liquidity, inflammability and electrochemical instability of liquid organic electrolyte [5,6], which are dangerous for cell operation. Therefore, efforts should be urged on the considerable challenge to find a safer and more sustainable electrolyte technology that would enable electric vehicles an extended driving range at high safety levels [7]. Solid-state electrolyte [8–11], including solid ceramic/polymer electrolyte and quasi-solid gel polymer electrolyte (GPE), is recognized as a rational substitute to offer one of the most promising approaches to withstand Li metal dendrites and improve safety [12]. However, many intrinsic drawbacks restrict its practical applications for solid ceramic/polymer electrolytes, including high impedance grain boundaries, interparticle interfacial resistance in compacted disks, difficult fabrication processes and insufficient ionic conductivities at room temperature [13,14].

To meet the above requirements, electrolytes that have good affinity with electrodes and ensuring high Li-ionic conductivity are urgently required. Gel polymer electrolyte consisting of polymer matrix with the liquid electrolyte being trapped [12,15,16], not only displays a much high ion conductivity and ease of fabrication, but also provides other benefits of improving safety by suppressing the formation of dendrite on the surface of lithium metal [14,16–19]. Some common polymers, such as poly(ethylene oxide) (PEO), poly(propylene oxide) (PPO), poly(acrylonitrile) (PAN) and poly(vinylidene fluoride hexafluoro propylene) (PVDF-HFP) could be used as matrices of GPE [16]. Among these polymer matrixes for GPE, PEO polymer, as a linear homopolymer, in particular is promising as host materials for preparing GPEs because the ether chain CH_2CH_2O unit in the PEO has strong interactions with lithium ions to provide paths for lithium ion transport well [11,12,16,20]. In addition, it also has other advantages including their low cost, reasonable mechanical stability, and excellent film-forming ability.

The electrolyte is the key component of any practical solid-state battery as well as the solid-state lithium–sulfur (Li–S) battery here under study [21]. “Quasi-solid-state” Li–S batteries (i.e., gel state, an

* Corresponding author.
E-mail addresses: tqian@suda.edu.cn (T. Qian), c.yan@suda.edu.cn (C. Yan).
[1] The two authors contributed equally to this work.

https://doi.org/10.1016/j.ensm.2019.01.024
Received 31 August 2018; Received in revised form 17 January 2019; Accepted 31 January 2019
Available online 01 February 2019
2405-8297/

intermediate state between liquid state and all solid state [12,15,16]) were developed, whose electrolytes (i.e., GPE) possess the hybrid characteristics combining polymer with liquid electrolytes. Liquid electrolyte could be well encapsulated in the GPE, thus high ionic conductivity and good affinity with electrodes could be obtained. In addition, the polymer matrix could effectively prevent leakage of liquid electrolyte thus improve safety of battery. We introduce a new type of super-high ionic conductive gel polymer (SHGP) electrolyte for greatly improved quasi-solid-state Li–S battery performance through a ring-opening polymerization reaction between poly(ethylene glycol) diglycidyl ether (PEGDE) and polyethylenimine, branched (PEI). The ether chain has strong interactions with lithium ions to provide paths for lithium ion transport well [11,12,16,20] and the lone-pair electrons of nitrogen from amino groups in the crosslinked polymer matrix could facilitate ionic transport by the formation of Li-ion coordinated bonds [22,23], thus leading to high lithium ion conductivity. DFT calculations and MD simulations theoretically confirmed that polar functional groups in the SHGP electrolyte could generate chemical interaction with lithium polysufides rather than just obstructing the polysulfides in physics, thus exhibiting strong adsorptivity to polysulfides, which is further verified by the experiments of visible adsorption and nucleation of Li_2S. Due to the aforementioned advantages of the SHGP electrolyte, the improved cycling performance for 400 cycle life was realized in a quasi-solid-state Li–S battery, which is far beyond that of pristine PEO. Furthermore, *in-situ* UV/Vis results throughout the entire cycling process displayed that the diffusion of polysulfides were effectively prohibited in the electrodes by using quasi-solid-state SHGP electrolyte.

2. Experimental section

2.1. The synthesis of the SHGP electrolyte

Poly(ethylene glycol) diglycidyl ether (PEGDE) and polyethylenimine, branched (PEI) was purchased from Alfa Aesar without any treatment. According to the scheduled molar fractions of epoxy groups in PEGDE and amino groups in PEI (1:1), the PEGDE and PEI were added in N,N-Dimethylformamide (DMF, from Aladdin) with the presence of LiTFSI as lithium salt (O/Li ratio of 8/1), the SHGP solution was then obtained. The solvent was evaporated for the fabrication of solid-state electrolyte membranes using a vacuum oven. The PEO electrolyte, which consists of PEO and the LiTFSI lithium salt with the O/Li ratio of 8/1 in acetonitrile (AN), was subjected to vigorous mixing via magnetic stirring to yield a uniform dispersion.

2.2. Characterization

Fourier transform infrared (FTIR) spectra were recorded on a Nicolet is50 spectrometer (ThemoFisher Scientific, America). X-ray photoelectron spectrometer (XPS, Kratos Axis Ultra Dld, Japan) was used to conduct surface elemental analysis performed. The morphology was observed by field emission scanning electron microscopy (FESEM, SU8010, Japan). Elemental analysis was conducted on an elementar (Vario Micro Cube, German). Thermogravimetric (TG) analysis was conducted on a thermal gravimetric analyzer (TG/DTA7300, SII NanoTechnology).

2.3. Electrochemical test

The S/C composite was obtained by heating the mixture of commercial sulfur powders (60 wt%) and carbon nanotube (40 wt%) at 155 °C for 24 h. Then, S/C and PVDF were dispersed with weight ratio of 9:1 in NMP solvent and then after grinding, the mixture was casted onto an aluminum current collector. After vacuum drying at 60 °C for 12 h, the composite cathode electrode was obtained. The cathode size is 1 cm^{-2}; the sulfur loading density could reach 2.5 mg cm^{-2}. Then, SHGP electrolyte membrane was coated on the prepared cathode electrode with an interfacial wetting of liquid organic electrolyte. The organic electrolyte used in the quasi-solid-state Li–S battery in this work is 1 M LiTFSI in 1,3-dioxolane (DOL) and dimethoxyethane (DME) mixture (1:1 in volume). 10 uL of the organic electrolyte was added as the gel-forming electrolyte. For comparison battery with PEO gel electrolyte was also prepared as noted above. The 2025 type coin cells using Li metal anode was assembled in the glove box. Cyclic voltammetry (CV) and electrochemical impedance spectroscopy (EIS) measurements were conducted on a CHI 660E electrochemical workstation (Chenhua Shanghai, China). The battery performance of cycling life and rate capability were tested within a voltage range of 1.5–2.8 V (vs. Li/Li^+) on battery testing system (LAND CT2001A, Wuhan, China) at room temperature.

2.4. Ion conductivity measurements

The ion conductivity measurements were performed on the CHI 660E electrochemical workstation (Chenhua Shanghai, China) by AC impedance spectroscopy using 2025 type coin cells sandwiching the SHGP and PEO electrolyte membrane wetted with organic electrolyte at the temperature range from 25 to 60°C between two stainless steel electrodes. Their lithium ionic conductivities were calculated from the EIS measurements according to the following equation:

$$\sigma = d/(R_b \cdot S) \quad (1)$$

Here, σ is for ionic conductivity, d is the thickness between two stainless steel electrodes, and S is the contact area between electrolyte and stainless steel electrode. R_b refers to the bulk resistance.

2.5. Electrolyte uptake study

Measurement of liquid uptake was carried out by dipping the polymeric film sample in the electrolyte solution [24]. The excess electrolyte remaining on the surface of the membrane was removed by wiping softly with a tissue paper. Sample was periodically weighed until no weight change was observed. The swelling ratio was defined by the weight ratio of the net liquid uptake to the dried polymer sample, can be written as

$$E = ((W_2 - W_1)/W_1) \times 100 \quad (2)$$

where, W_1 andW_2 are the mass of the membranes before and after dipping in the electrolyte solution, respectively.

2.6. Synthesis of Li_2S_8 solution

The stoichiometric amounts of sulfur and lithium sulfide with molar ratio of 7:1 were dissolved in 1 M LiTFSI, followed by vigorous magnetic stirring for 24 h thus yielding a deep red solution. The concentration of the Li_2S_8 solution was 20 mM. It should be noted that the whole synthesis procedure was carried out in argon gas-filled glove box.

2.7. Polysulfide visible adsorption test

The same quality of PEO and SHGP membrane was separately covered the bottom of tube. The sample vial was filled with blank electrolyte, and Li_2S_8 solution was injected into a plastic tube with small holes at the bottom inside the vial. The discoloration was recorded by standing different hours.

2.8. Nucleation of Li_2S test

Here, an electronically conductive material of carbon nanotubes was used to offer a substrate for the electrodeposition reactions. The SHGP and PEO were fabricated into the conductive substrate respec-

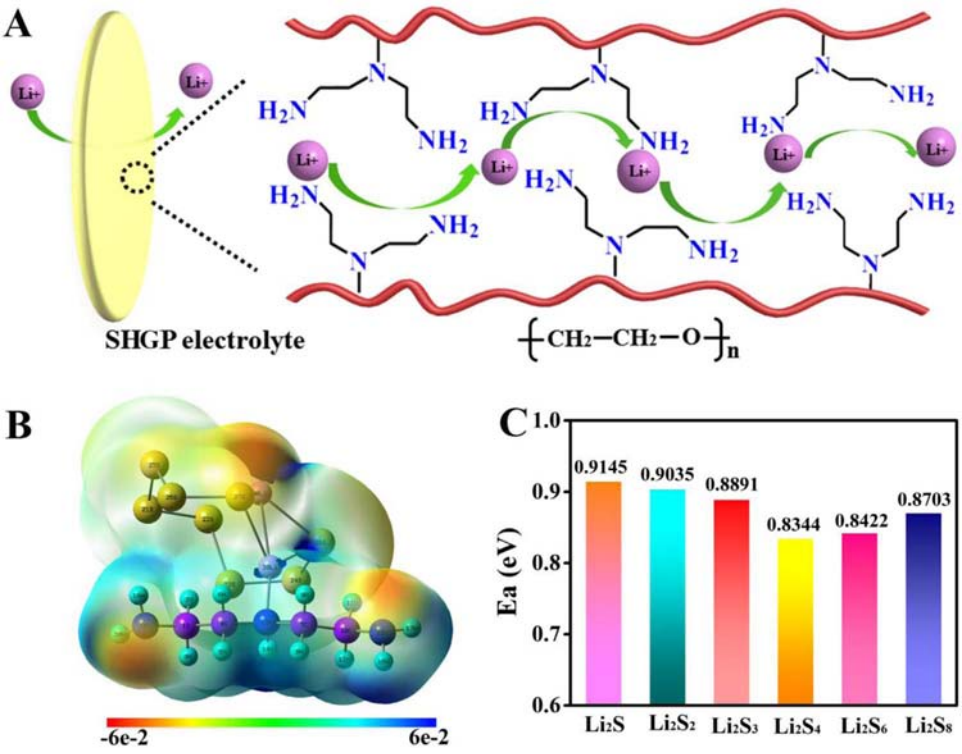

Fig. 1. (A) The schematic illustration and the working principle of high ionic conductive SHGP gel electrolyte. (B) Probability of electron cloud density distribution of Li–S composites on a reducible molecular structure of SHGP. N: blue; C: purple; H: cyan; Li: pink; S: yellow. (C) The exact adsorption binding energies at six different lithiation stages (Li_2S, Li_2S_2, Li_2S_3, Li_2S_4, Li_2S_6, and Li_2S_8).

tively for comparison. Blank electrolyte of 20 μL was dropped onto the lithium foil anode and 20 μL Li_2S_8 catholyte was added in the compartment. The cells were discharged galvanostatically at 0.112 mA to 2.06 V and then kept potentiostatically at 2.05 V for lithium sulfides to nucleate and grow. Potentiostatic discharge was ceased when the current was below 10^{-5} A.

2.9. *In-situ UV/Vis spectra measurements*

The *in-situ* UV/Vis test was conducted to determine the polysulfide concentration at the anode side which shuttled from the cathode side. For *in-situ* UV/Vis spectra measurements (UV-2450, Shimadzu corporation, Japan), the lithium anode was punched into a ring and the cell shell is equipped with a sealed glass cover. The UV/Vis could traverse the glass cover and there was no lithium present between the glass cover and the cathode; therefore, the UV/Vis spectra could detect whether there were polysulfides transferred to the anode side from cathode side. With the discharging time went on, the changes of polysulfide concentration at the anode side could be recorded.

2.10. *Computational method*

The rb3lyp density functional method was employed in this work to carry out all the computations. All the atoms were simulated by using the 6-31G (d+p) [25] basis set. Vibrational frequency analyses at the same level of theory were performed on all optimized structures to characterize stationary points as local minima or transition states. The Gaussian 09 suite of programs was used throughout. The adsorption binding energy was computed to measure the adsorption binding energies (E_a) of Li_2S_n (Li_2S, Li_2S_2, Li_2S_3, Li_2S_4, Li_2S_6, Li_2S_8) species (E_{Li2Sn}) and the reducible molecular structures of different polymer matrix ($E_{polymer}$). It was defined as the energy difference between the adsorbed polmer/Li_2S_n system ($E_{Li2Sn+polymer}$) and the simple summation of isolated Li_2S_n species and polymer can be expressed as $E_a = E_{Li2Sn} + E_{polymer} - E_{Li2Sn+polymer}$. With this definition, a positive binding energy indicated that the binding interaction was favored.

MD simulations were performed with Gromacs, v5.0.5. The simulation system was constructed by dissolving SHGP polymer matrix (PEO and PEI segments) or PEO polymer matrix (PEO segment), 50 LiTFSI molecules and 50 Li_2S_8 molecules into the solvent (358 DOL + 243 DME molecules). Regarding the force field parameterization, the SHGP/PEO/DME/DOL molecules were simulated by the OPLS-AA force field, and Li_2S_8 and LiTFSI were parameterized according to previous studies [26–28]. Calculation of the interatomic interactions consists of two parts, i.e., the Van der Waals (VDW) interactions and coulombic interactions. The VDW interactions were represented by the Lennard Jones (LJ) potential with a cut off value at 1.2 nm, with the geometric combination rule to calculate the LJ parameters for unlike atom pairs, i.e., $\sigma_{ij}=(\sigma_i\sigma_j)^{1/2}$ and $\varepsilon_{ij}=(\varepsilon_i\varepsilon_j)^{1/2}$. Coulombic interactions were calculated with the particle mesh Ewald algorithm, with the short-range part truncated at 1.2 nm and the long-range part calculated in the reciprocal space with a Fourier spacing of 0.12 nm. The equations of motion during simulations were integrated by the leap-frog algorithm with a time-step of 1 fs. Energy minimization with the steepest descent algorithm was carried out to avoid bad contacts during model construction, followed by isothermal-isobaric equilibration at 298.15 K/1 bar for 50 ps. Subsequently, production runs were carried out under NPT ensemble (constant number of atoms, constant temperature with the Nose-Hoover thermostat and constant pressure with the Parrinello-Rahman barostat) for 20 ns. Three dimensional periodic boundary conditions were applied through all simulation runs.

3. Results and discussions

The schematic illustration and the working principle of the SHGP electrolyte were shown in Fig. 1A. The SHGP molecular structure featured with polar nitrogen heteroatoms [22,23] and ether chains [11,12,16,20] could benefit for lithium ion transport because they could coordinate with lithium ions. Therefore, the whole electrolyte system combined liquid phase and SHGP matrix would together

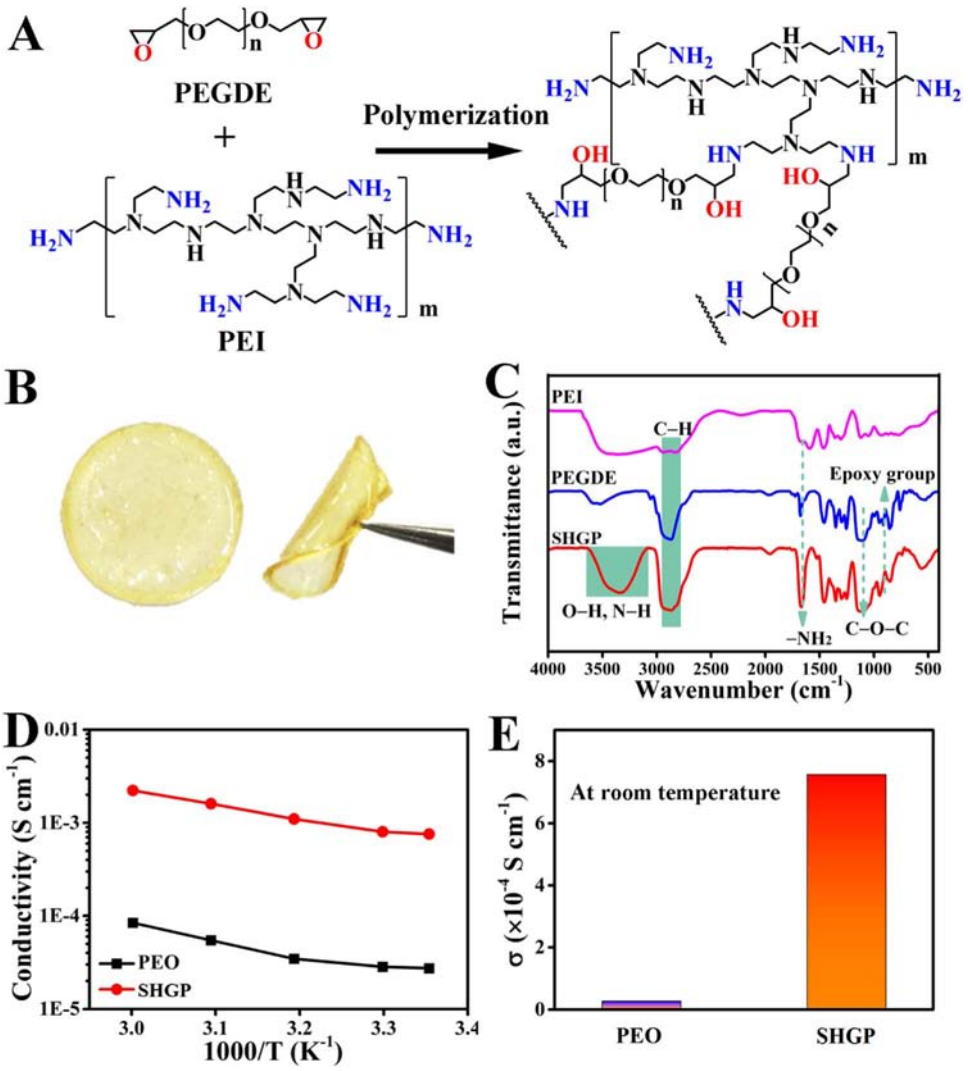

Fig. 2. (A) Synthesis scheme of the polar polymer by polymerization of PEGDE and PEI. (B) The optical photograph exhibits the flexibility and elasticity of the synthetic polar gel polymer. (C) The FTIR spectra of PEI, PEGDE and SHGP. (D) Ionic conductivities for the SHGP electrolyte and PEO gel polymer at various temperatures and (E) at room temperature.

contribute to the fast lithium ion motions [29]. On the other hand, the polar functional groups in SHGP could exhibit strong adsorptivity and immobilization to the dissolved lithium polysulfides [30–32] through chemical adsorption [33,34]. Therefore, lithium polysulfide molecules are preferentially immobilized rightly on the interface of SHGP contacted with sulfur cathode rather than diffuse into the electrolytes and away from electrodes. To better understand the mechanism, the adsorption binding strength between the SHGP electrolyte and discharge products of Li_2S_n ($1 \le n \le 8$) intermediates were investigated by DFT calculations (Fig. 1B). The high values of the adsorption binding energies at six different lithiation stages on SHGP electrolyte are listed in Fig. 1C, verifying that the functional SHGP electrolyte can effectively anchor different Li_2S_n species. Affinity between polymer electrolytes including PEO, PAN and PVDF-HFP and the lithium atoms in lithium polysulfides were all calculated and demonstrated in Fig. S1. Clearly, the adsorption binding energies for SHGP with lithium polysulfides are the largest among these polymers.

The ring-opening polymerization reaction between PEGDE and PEI was demonstrated in Fig. 2A, implying that the reaction between the amino groups in PEI with the epoxy groups in PEGDE [35] leads to the formation of the polar gel polymer (Fig. 2B). The LiTFSI was fully dissolved and uniformly distributed in the SHGP matrix as the obtained SHGP polymer was transparent as shown in Fig. S2. TG analysis was also conducted to confirm that there is no any residual solvent in the SHGP membrane (Fig. S3). FTIR spectroscopy (Fig. 2C) elucidated the structural changes before and after polymerization. The peak at 1110 cm^{-1} is assigned to the C–O–C stretching in the ether chain CH_2CH_2O unit [12] and the peak at 1650 cm^{-1} is assigned to the bending vibrations of N–H [36]. The broad peak 3650–3082 cm^{-1} is attributed to the stretching vibration of O–H and N–H [37]. After reaction, the peak corresponding to epoxy stretching [12] at 900 cm^{-1} disappears in the spectrum, which validates the successful reactions between the amino groups in PEI with the epoxy groups in PEGDE to form a polymer framework. In addition, X-ray photoelectron spectroscopy (XPS) measurement was also conducted to elaborate the chemical bonding configurations in the formed polymer. According to the full XPS survey spectrum (Fig. S4A), predominant peaks of C1s, N1s and O1s all existed. From the high-resolution C1s XPS spectra (Fig. S4B), four peaks can be identified at 285.1 eV assigned to sp^3 C (C–C) [38, at 285.8 eV assigned to C–N [39], at 286.2 eV assigned to C–OH and at 286.5 eV assigned to C–O dans poly(ethylene glycol) (PEG) [38]. As shown in Fig. S4D, three peaks of N1s located at ~399.7, ~399.1 eV and 398.6 eV, corresponding to the tertiary amines, C–N and primary amines respectively [36], were detected. In the meantime, the presence of C–OH bond was also confirmed by the O1s XPS spectra in Fig. S4C [38]. Therefore, the occurrence of polymerization reaction between the amino groups in PEI with the epoxy groups in PEGDE is further verified by the clear XPS results.

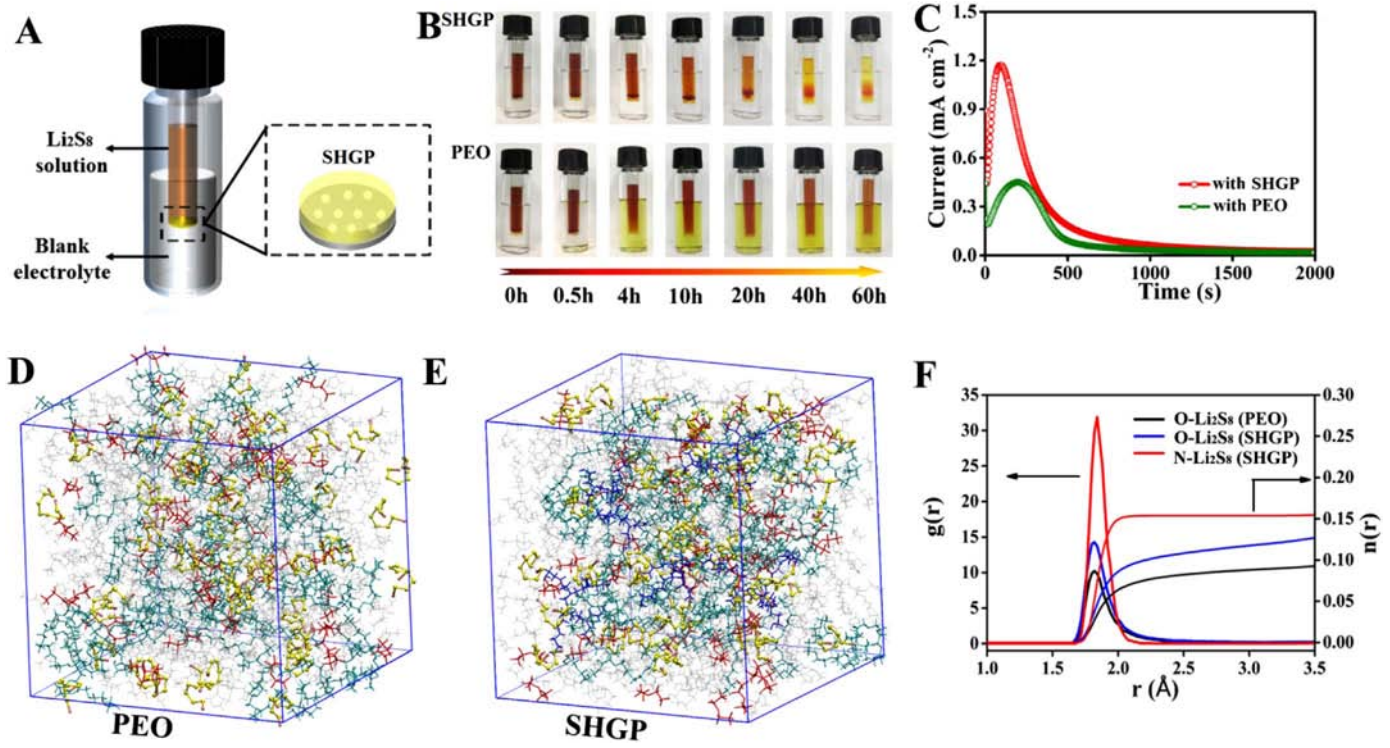

Fig. 3. (A) Schematic of visual experiments. The blank electrolyte is 1 M LiTFSI in DOL and DME (1:1 in volume). (B) Visual comparison of adsorptivity of SHGP and PEO to Li_2S_8. (C) Potentiostatic discharge curves at 2.08 V for Li_2S deposition with SHGP and PEO respectively. MD simulations for Li_2S_8 (D) in PEO and (E) in SHGP. LiTFSI: red; DOL/DME: grey; PEO segment: teal; PEI segment: blue; Li_2S_8: yellow. (F) Li_2S_8 radial distribution functions in PEO and SHGP.

The lithium ion conductivity of the SHGP electrolyte and PEO gel polymer were also measured by AC impedance [5,18]. It was clear that the ionic conductivity increases with an increase in temperature and higher lithium conductivity was obtained for the SHGP electrolyte than that of PEO gel polymer (Fig. 2D). Specially, the ionic conductivity for the SHGP electrolyte at room temperature was 0.75 mS cm^{-1} (Fig. 2E), which is comparable to that of liquid electrolyte and would lead to the rapid transport of Li^+ on discharge–charge stage. The liquid electrolyte could be well encapsulated into SHGP polymer matrix (Fig. S5). In addition, the lone-pair electrons on the oxygen of the ether groups and the nitrogen of the amino groups can coordinate lithium ions, which are beneficial for ionic transport, as discussed in Fig. 1A. Therefore, the whole electrolyte system combined liquid phase and SHGP matrix would together contribute to the fast lithium ion motions.

The strong anchoring of polysulfides by the SHGP was confirmed through visible adsorption of 20 mM Li_2S_8 [40]. Fig. 3B gives a conspicuous visual comparison of adsorptivity to polysulfides of the SHGP and PEO by a well-designed device in Fig. 3A. The sample vial was filled with blank electrolyte, and Li_2S_8 solution was injected into a plastic tube with small holes at the bottom inside the vial. The blank electrolyte is 1 M LiTFSI in DOL and DME (1:1 in volume). The polymers PEO and SHGP at the bottom of tube were all 20 mg. For the SHGP, Li_2S_8 solution in the plastic tube exhibits a stronger decolorization and a significant dark red appeared at the interface of Li_2S_8 solution and the polymer SHGP. In addition, the blank solution keeps colorless all the time. These phenomena indicate that Li_2S_8 was effectively adsorbed and could not pass through the SHGP. In contrast, the Li_2S_8 was easier to permeate through the pristine PEO polymer thus the color of blank electrolyte was changed to be bright yellow within a short time. Furthermore, the color fading of Li_2S_8 solution was slower than that for SHGP because the pristine PEO could not greatly adsorb Li_2S_8 as the SHGP. The states of blank electrolyte in the sample vial as function of time were recorded by the UV–vis measurement (Fig. S6). The absorbance of electrolyte in the sample vial for PEO polymer kept growing as time went by because the Li_2S_8 was easy to permeate through the pristine PEO polymer, while nearly no absorbance change of electrolyte was observed in the sample vial for SHGP polymer. The significant comparison convinces that polymer SHGP has an incomparable superiority in trapping Li_2S_8, which are important characteristics for GPE in Li–S batteries. S 2p XPS characterization for the polysulfides trapped by the SHGP from Fig. 3B was conducted as shown in Fig. S7. Except signals representing LiTFSI and polysulfides, no other signals were detected. This indicated polysulfides trapped by the polymer electrolyte are still anchored polysulfide molecules without reaction between the polymer. In addition, the effect of SHGP as efficient blockage for polysulfide migration was attested by the permeation test in Fig. S8. In this simulation experiment, the polysulfides scarcely exhibited any infiltration in SHGP even after 24 hours of placement. On the contrary, it was apparent that polysulfides permeated and diffused into the electrolytes severely, indicating its lower resistance to the diffusion of polysulfides.

The strong adsorption to polysulfides would favor the interfacial polysulfide redox and Li_2S deposition [32,41]. Thus, we monitored the kinetics of Li_2S nucleation by potentiostatically discharging Li_2S_8 catholyte. An electronically conductive material of carbon nanotubes was used to provide a substrate for the electrodeposition reactions [32,41]. Further, the SHGP and PEO were fabricated into the conductive substrate respectively for comparison. Blank electrolyte of 20 μL was dropped onto the lithium foil anode and 20 μL Li_2S_8 catholyte was added in the compartment. The cells were discharged galvanostatically at 0.112 mA to 2.06 V and then kept potentiostatically at 2.05 V for lithium sulfides to nucleate and grow. Potentiostatic discharge was ceased when the current was below 10^{-5} A. As shown in Fig. 3C, the cell with SHGP exhibits a much stronger current peak than that with PEO, indicating a higher affinity to Li_2S_8 and efficient deposition of Li_2S attributed to the abundant nucleation sites arisen from enriched polar functional groups. The bond lengths between the lithium atoms in six different lithium polysulfides and the nitrogen atoms on a reducible molecular structure of SHGP were also demonstrated in Fig. S9. Due to the energy and structure differences of different Li_2S_n species and

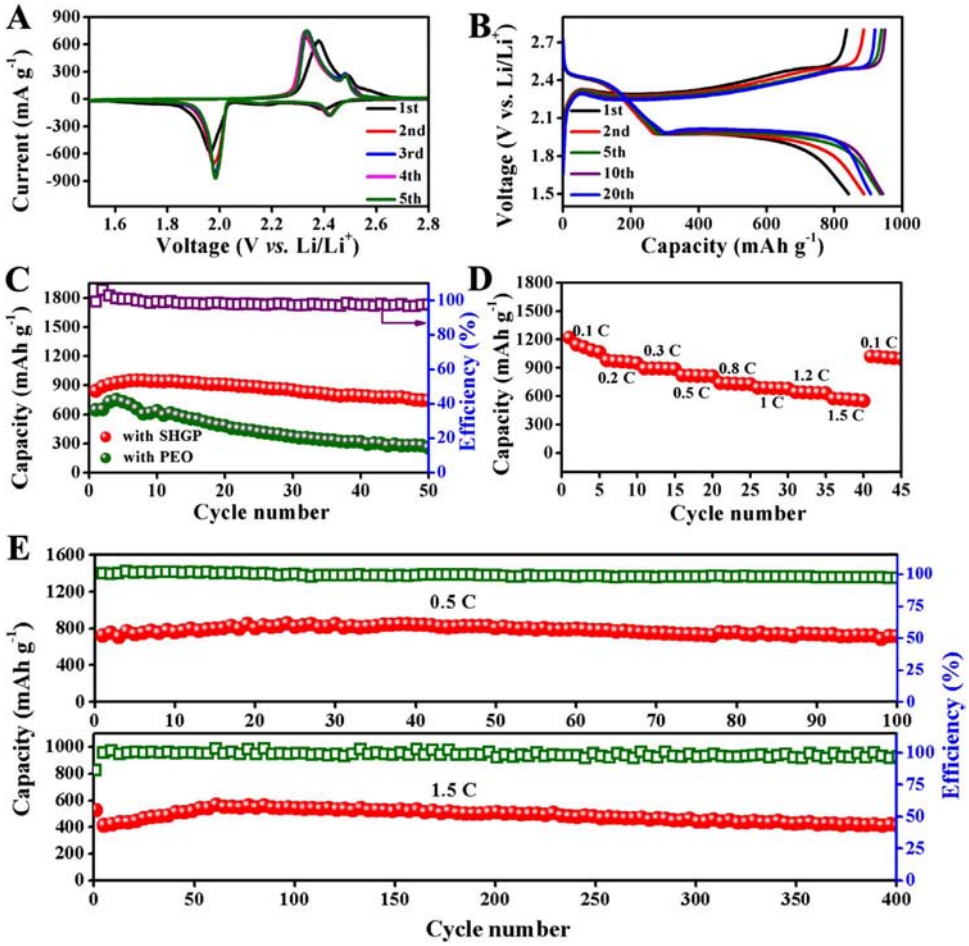

Fig. 4. (A) CV profiles at a scan rate of 0.02 mV s^{-1} in a potential window from 1.5 to 2.8 V and (B) Discharge/charge voltage profiles at 0.2 C of Li–S battery with SHGP electrolyte. (C) Comparison of cycling performance of Li–S battery with SHGP electrolyte and with PEO tested at a current rate of 0.2 C. (D) Rate performance and (E) cycling performance at a current rate of 0.5 C and 1.5 C of solid state Li–S battery with SHGP electrolyte.

SHGP/Li_2S_n adsorbed systems (n=1, 2, 3, 4, 6, 8), the variations of bond lengths between lithium atoms in six different Li_2S_n (Li_2S, Li_2S_2, Li_2S_3, Li_2S_4, Li_2S_6, and Li_2S_8) and the nitrogen atoms on a reducible molecular structure of SHGP could be observed. In addition, other effects from all components in the GPE system are nonnegligible. Therefore, MD simulations for Li_2S_8 molecules and the whole GPE systems including polymer matrix, salt (LiTFSI) and organic solvents (DOL and DME) were conducted. Intuitionistic vision effects from Fig. 3D and Fig. 3E are apparent that Li_2S_8 molecules tend to concentrate near the polymer matrix of SHGP (Fig. 3E) rather than distribute randomly in PEO-based GPE (Fig. 3D). In addition, radial distribution functions (RDF) and integrated RDF for O–Li_2S_8 in PEO, O–Li_2S_8 and N–Li_2S_8 in SHGP were also calculated as shown in Fig. 3F, confirming that the enriched polar functional amino groups derived from PEI are helpful indeed for adsorption and immobilization of lithium polysulfides.

We then assessed the electrochemical performance of Li–S cells with the SHGP electrolyte. Fig. 4A depicted the cyclic voltammetry (CV) curves scanned at 0.02 mV s^{-1} for the initial five cycles in the potential range of 1.5–2.8 V. In the first cathodic scan, the reduction peaks centered at 2.39 V and 1.96 V corresponds to the reduction of sulfur to high-order polysulfides and then to sulfides. The two adjacent oxidation peaks at 2.38 and 2.48 V in the subsequent anodic sweep are attributed to the conversion of lithium sulfide to polysulfides and then to sulfur [8,42]. And then, the subsequent CV curves show no changes in the CV peak positions or peak current, confirming the good electrochemical stability of Li–S cells with SHGP by efficiently trapping the soluble polysulfides. Consistent results were also garnered from the stable and overlapping charge/discharge plateaus in the galvanostatic charge/discharge profiles at 0.2 C (1C=1675 mA g^{-1}, Fig. 4B) and the cycling performance at 0.2 C reconfirm the superior cyclability (Fig. 4C). Instead, the battery performance only with pristine PEO rapidly deteriorated. Fig. 4D presents the specific capacities at different current rates. The cell delivers discharge capacities of 1110 mA h g^{-1} at a current rate of 0.1 C and a high capacity at high rate of 1.5 C. Then, the current rate abruptly returns to 0.1 C, a reversible capacity of 1010 mAh g^{-1} can also be obtained. The cycle performance was also electrochemically characterized by monitoring the discharge capacity using different current densities of 0.5 C and 1.5 C-rate for charging and discharging (Fig. 4E). At a lower rate of 0.5 C, it delivers an initial capacity of 720 mAh g^{-1}, and increases to 850 mAh g^{-1}. After 100 cycles, a reversible capacity of 715 mAh g^{-1} is obtained, with capacity retention of 98 % and a high Coulombic efficiency of ~100 %. The cyclability at 1.5 C rate still remains a retention rate of 85 % after 400 cycles. Furthermore, the issue of lithium dendrites generation and Li_2S deposition on lithium anodes originating from the repeated stripping/plating of a lithium layer and the shuttle effect of soluble polysulfides should be emphasized as the formation of uniform and stable solid-electrolyte interphase (SEI) layer is essential to ensure good electrochemical performance in Li–S batteries [43]. Scanning Electron Microscopy (SEM) images of superficial morphology of lithium foil anodes for the quasi-solid-state Li–S batteries with SHGP and PEO as gel electrolyte after 50 discharging/charging were demonstrated in Fig. S10. Smooth top surface of the lithium foil without obvious growth of

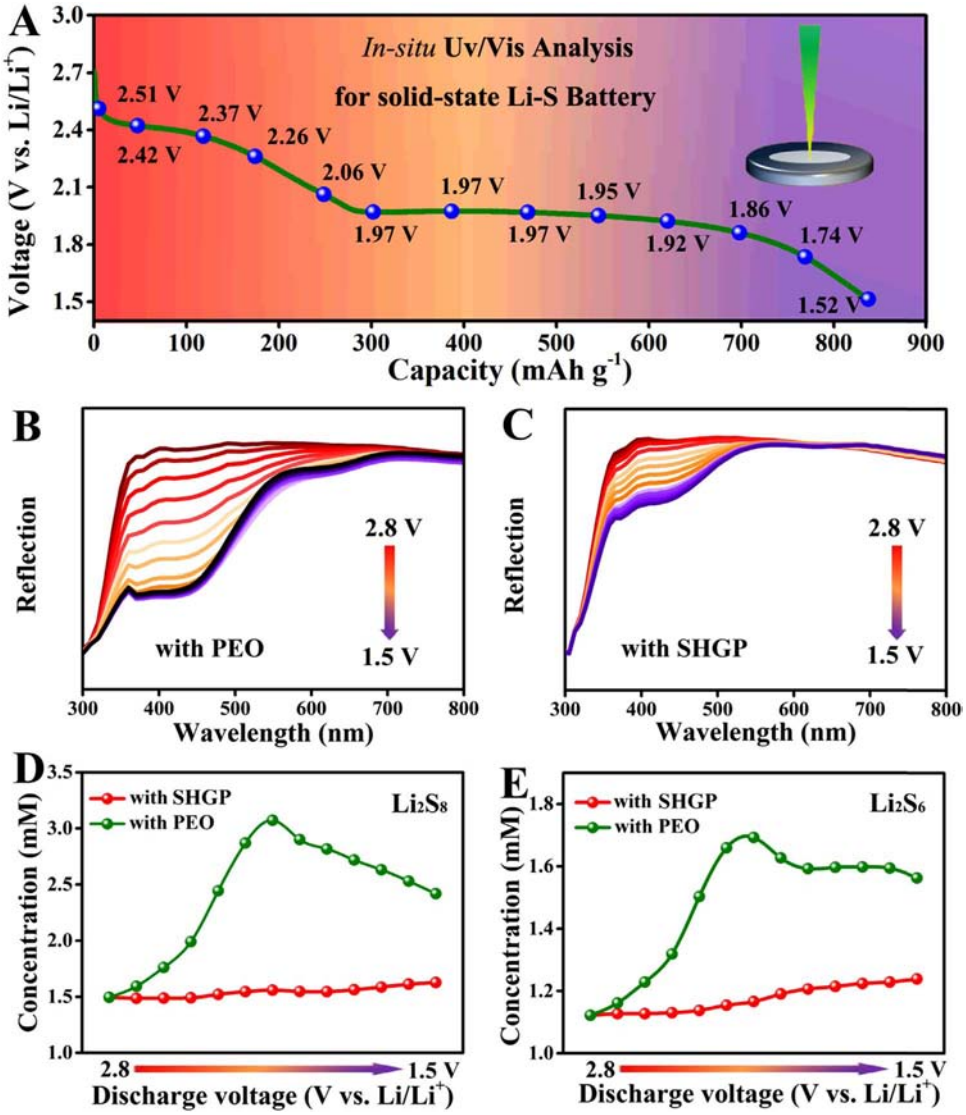

Fig. 5. The *in-situ* UV/Vis spectra of discharging batteries assembled with (B) PEO and (C) SHGP electrolyte between λ = 300 to 800 nm. Derived from the UV/Vis spectra, the polysulfide concentrations of (D) Li_2S_8, (E) Li_2S_6 at the anode side at different potentials in different cells corresponding to (A) the voltage changes.

lithium dendrites can be observed for SHGP cell (Fig. S10A). However, some rough lithium dendrites and Li_2S by-product (Fig. S10B) on the lithium anode of PEO cell was revealed, indicating that the synthesized polar polymer used as SHGP electrolyte for solid-state Li–S batteries could greatly suppress the generation of dendrites and the deposition Li_2S. Furthermore, surface morphologies of sulfur cathodes after cycling were investigated to confirm the integrity and stability of sulfur electrode surfaces [33] in Fig. S11. Massive sulfur species dendrites derived from irreversible polysulfides grew on the surface of sulfur electrode in PEO gel polymer (Fig. S11D). Conversely, the surface of sulfur electrode in SHGP maintained integrated GPE/electrode interface with a smooth morphology and no sulfur species dendrites (Fig. S11B). Elemental analysis was also conducted for the cycled cathode ended with charged state. The cathode was rinsed by DME then dried. About 98% sulfur amount could be maintained, indicating high sulfur utilization during cycling. In addition, the changes of SHGP electrolytes were investigated by XPS measurements before and after cycling ended with charged state (Fig. S12). The changes in the C 1s and F 1s XPS spectra could be ascribed to that the liquid organic electrolytes were consumed in the initial cycles due to the SEI formation. Beyond that, no other changes took place in the SHGP electrolytes before and after cycling.

Electrochemical impedance spectroscopy (EIS) measurements were carried out to gain further insight into the electrochemical characteristics [44]. The impedance spectra (Fig. S13) displayed two depressed semicircles at both the high (HF) and middle frequency (MF) range. The depressed semicircle in the HF region may reflect the charge transfer process (R_{CT1}) at the conductive agent interface, and the depressed semicircle in the MF range may be attributed to the formation of insoluble polysulfide species (R_{CT2}) [45]. With discharging/charging going on, stable reaction kinetics derived from the built interfacial SEI film was obtained thus the charge transfer resistance in the EIS plots (Fig. S13) gradually stabilized. In addition, the lithium ion diffusion coefficient (D_{Li^+}) of the cells with SHGP electrolyte is also investigated. CV analysis (Fig. S14A) was conducted to evaluate the D_{Li^+} using the Randles–Sevcik equation, as described below,

$$I_p = 2.69 \times 10^5 n^{1.5} A D_{Li^+}^{+0.5} v^{0.5} C_{Li+} \quad (3)$$

where I_p indicates the peak current (A), n is the number of electrons in the reaction, A is the electrode area (cm^{-2}), v is the scan rate ($V\ s^{-1}$), and C_{Li^+} is the lithium-ion concentration in the electrolyte ($mol\ cm^{-3}$) [43,46,47]. From the linear relationship of I_p and $v^{0.5}$ (Fig. S14B), D_{Li^+} for peak A and C were calculated to be 2.5×10^{-8} and 5.2×10^{-9} $cm^2\ s^{-1}$.

It is worth noting that D_{Li}^{+} for the two redox peaks of the battery with SHGP electrolyte was comparable to that of other sulfur-based cathodes [47,48], suggesting that the SHGP would not hinder fast Li-ion transport. The good lithium ion diffusion is reasonable considering the high lithium conductivity of SHGP electrolyte as discussed above.

To identify whether there were polysulfides transferred to the anode side and extract the information of discharge products of polysulfides species at the anode side during discharging in real time, an effective tool by using *in-situ* UV/vis spectroscopy measurements was conducted according to the depths of discharge marked by different colors [40,43,49]. The measured UV/Vis spectra of Li–S batteries assembled with PEO and SHGP electrolyte are shown in Fig. 5B and C, respectively. As shown in the UV/vis spectra of battery with PEO of Fig. 5B, the formation of long-chain polysulfides was detected as reflectance values undergoes apparent and quick decline upon discharging at higher wavelengths. Along with further discharging, the absorbance shifts towards shorter wavelengths was observed, indicating the conversion from long-chain polysulfides to short-chains, which is a common phenomenon for Li–S batteries. However, the only difference between batteries with PEO and SHGP electrolyte was that the spectra in Fig. 5C show almost no change in the reflection towards the higher wavelengths and the reflection changes were demonstrated to be much weaker than that of battery with PEO, implying that the SHGP has significant influence on adsorption and immobilization for polysulfides. Furthermore, quantitative determination of different polysulfides at the anode side [40,49,50] was conducted to clearly explain the changes of polysulfide concentration at the anode side in different cells corresponding to the voltage change (Fig. 5A). Fig. 5D showed the changes of concentration for Li_2S_8 at the anode side of two cells as the discharging goes on. It could be clearly observed that the release of Li_2S_8 from the electrode in cell with PEO was much faster than that with SHGP. At the beginning of discharging, the concentration values of Li_2S_8 was at the same level in different cells, but a significant increase of concentration at the anode side of the cell with PEO was displayed very soon. On the contrary, the concentration of Li_2S_8 at the anode side of cell with SHGP electrolyte was maintained at an almost constant value in the whole discharging process. The similar results can be observed for Li_2S_6 in Fig. 5E, indicating that most of polysulfides were fixed into the electrodes by multiple polar functional groups of the SHGP thus there were few polysulfides released.

4. Conclusion

In summary, we proposed a new super-high ionic conductive polymer (SHGP) electrolyte (2.2×10^{-3} S cm^{-1} at 60 °C and 0.75×10^{-3} S cm^{-1} at 30 °C), which enabled us to achieve a high specific capacity of 950 mAh g^{-1} at 0.2 C and superior capacity retention of ~98 % after 100 cycles at 0.5 C, far beyond that of conventional PEO gel electrolyte for quasi-solid-state Li–S battery. The SHGP electrolyte exhibited strong adsorptivity to lithium polysulfides as the enriched polar functional groups in SHGP could generate chemical adsorption with lithium polysufides, which was theoretically confirmed by DFT calculations and MD simulations. The visual characterizations and experiment of nucleation of Li_2S give direct evidence on the good affinity of SHGP to Li_2S_8 that was confirmed by *in-situ* UV/Vis spectroscopy, indicating the long-chain polysulfides were fixed with the affluent polar functional groups of the SHGP. Undoubtedly, the original design of this super-high ionic conductive polymer electrolyte demonstrated here opens a new direction in high performance quasi-solid-state Li–S batteries.

Acknowledgment

We acknowledge the support from the National Natural Science Foundation of China (No. 51622208, No. 21703149), and the Priority Academic Program Development of Jiangsu Higher Education Institutions (PAPD).

Appendix A. Supporting information

Supplementary data associated with this article can be found in the online version at doi:10.1016/j.ensm.2019.01.024.

References

[1] E. Quartarone, P. Mustarelli, Chem. Soc. Rev. 40 (2011) 2525–2540.
[2] N. Ohta, K. Takada, L.Q. Zhang, R.Z. Ma, M. Osada, T. Sasaki, Adv. Mater. 18 (2006) 2226–2229.
[3] Y. Lin, X.M. Wang, J. Liu, J.D. Miller, Nano Energy 31 (2017) 478–485.
[4] A. Unemoto, S. Yasaku, G. Nogami, M. Tazawa, M. Taniguchi, M. Matsuo, T. Ikeshoji, S. Orimo, Appl. Phys. Lett. 105 (2014) 083901.
[5] X.Y. Tao, Y.Y. Liu, W. Liu, G.M. Zhou, J. Zhao, D.C. Lin, C.X. Zu, O.W. Sheng, W.K. Zhang, H.W. Lee, Y. Cui, Nano Lett. 17 (2017) 2967–2972.
[6] P.G. Bruce, S.A. Freunberger, L.J. Hardwick, J.M. Tarascon, Nat. Mater. 11 (2012) 19–30.
[7] W. Liu, S. Lee, D.C. Lin, F.F. Shi, S. Wang, A.D. Sendek, Y. Cui, Nat. Energy 2 (2017) 17035.
[8] A. Manthiram, Y.Z. Fu, S.H. Chung, C.X. Zu, Y.S. Su, Chem. Rev. 114 (2014) 11751–11787.
[9] Y. Zhao, Y.G. Zhang, D. Gosselink, T.N.L. Doan, M. Sadhu, H.J. Cheang, P. Chen, Membranes 2 (2012) 553–564.
[10] L. Chen, L.Z. Fan, Energy Storage Mater. 15 (2018) 37–45.
[11] Y. Lin, J. Li, K. Liu, Y.X. Liu, J. Liu, X.M. Wang, Green Chem. 18 (2016) 3796–3803.
[12] Q.W. Lu, Y.B. He, Q.P. Yu, B.H. Li, Y.V. Kaneti, Y.W. Yao, F.Y. Kang, Q.H. Yang, Adv. Mater. 29 (2017) 1604460.
[13] W.D. Zhou, S.F. Wang, Y.T. Li, S. Xin, A. Manthiram, J.B. Goodenough, J. Am. Chem. Soc. 138 (2016) 9385–9388.
[14] J. Shim, H.J. Kim, B.G. Kim, Y.S. Kim, D.G. Kim, J.C. Lee, Energy Environ. Sci. 10 (2017) 1911–1916.
[15] J.Z. Guo, A.B. Yang, Z.Y. Gu, X.L. Wu, W.L. Pang, Q.L. Ning, W.H. Li, J.P. Zhang, Z.M. Su, ACS Appl. Mater. Interfaces 10 (2018) 17903–17910.
[16] W.W. Huang, Z.Q. Zhu, L.J. Wang, S.W. Wang, H. Li, Z.L. Tao, J.F. Shi, L.H. Guan, J. Chen, Angew. Chem. , Int. Ed. 52 (2013) 9162–9166.
[17] J.I. Kim, Y. Choi, K.Y. Chung, J.H. Park, Adv. Funct. Mater. 27 (2017) 1701768.
[18] C. Li, Z.Y. Guo, B.C. Yang, Y. Liu, Y.G. Wang, Y.Y. Xia, Angew. Chem. Int. Ed. 56 (2017) 9126–9130.
[19] Q.S. Wang, Z.Y. Wen, J. Jin, J. Guo, X. Huang, J.H. Yang, C.H. Chen, Chem. Commun. 52 (2016) 1637–1640.
[20] J.M. Sarapas, G.N. Tew, Macromolecules 49 (2016) 1154–1162.
[21] W. Yang, W. Yang, J.N. Feng, Z.P. Ma, G.J. Shao, Electrochim. Acta 210 (2016) 71–78.
[22] Y.X. Tang, J.Y. Deng, W.L. Li, O.I. Malyi, Y.Y. Zhang, X.R. Zhou, S.W. Pan, J.Q. Wei, Y.R. Cai, Z. Chen, X.D. Chen, Adv. Mater. 29 (2017) 1701828.
[23] J. Liu, Q. Zhang, T. Zhang, J.T. Li, L. Huang, S.G. Sun, Adv. Funct. Mater. 25 (2015) 3599–3605.
[24] S. Choudhury, T. Saha, K. Naskar, M. Stamm, G. Heinrich, A. Das, Polymer 112 (2017) 447–456.
[25] M.J. Frisch, et al., G.W. Trucks, H.B. Schlegel, G.E. Scuseria, M.A. Robb, J.R. Cheeseman, G. Scalmani, V. Barone, B. Mennucci, G.A. Petersson, Gaussian 09, Revision C.01, Gaussian, Inc., Wallingford CT, 2010.
[26] N.N. Rajput, V. Murugesan, Y. Shin, K.S. Han, K.C. Lau, J.Z. Chen, J. Liu, L.A. Curtiss, K.T. Mueller, K.A. Persson, Chem. Mater. 29 (2017) 3375–3379.
[27] J.C. Soetens, C. Millot, B. Maigret, J. Phys. Chem. A 102 (1998) 7.
[28] J.C. Lopes, A.A.H. Pa´dua, J. Phys. Chem. B 108 (2004) 16893–16898.
[29] X.B. Cheng, C. Yan, X.Q. Zhang, H. Liu, Q. Zhang, ACS Energy Lett. 3 (2018) 1564–1570.
[30] Z.Y. Wang, Y.F. Dong, H.J. Li, Z.B. Zhao, H.B. Wu, C. Hao, S.H. Liu, J.S. Qiu, X.W. (David) Lou, Nat. Commun. 5 (2014) 5002.
[31] J.X. Song, M.L. Gordin, T. Xu, S.R. Chen, Z.X. Yu, H. Sohn, J. Lu, Y. Ren, Y.H. Duan, D.H. Wang, Angew. Chem. 127 (2015) 4399–4403.
[32] C.Y. Chen, H.J. Peng, T.Z. Hou, P.Y. Zhai, B.Q. Li, C. Tang, W.C. Zhu, J.Q. Huang, Q. Zhang, Adv. Mater. 29 (2017) 1606802.
[33] M. Liu, D. Zhou, Y.B. He, Y.Z. Fu, X.Y. Qin, C. Miao, H.D. Du, B.H. Li, Q.H. Yang, Z.Q. Lin, T.S. Zhao, F.Y. Kang, Nano Energy 22 (2016) 278–289.
[34] D. Zhou, Y. Chen, B.H. Li, H.B. Fan, F.L. Cheng, D. Shanmukaraj, T. Rojo, M. Armand, G.X. Wang, Angew. Chem. Int. Ed. 57 (2018) 10168–10172.
[35] S. Quan, S.W. Li, Z.X. Wang, X.R. Yan, Z.H. Guo, L. Shao, J. Mater. Chem. A 3 (2015) 13758–13766.
[36] W.F. Zhang, S.S. Wang, J.Y. Ji, Y. Li, G.L. Zhang, F.B. Zhang, X.B. Fan, Nanoscale 5 (2013) 6030–6033.
[37] G.I. Dovbeshko, N.Y. Gridina, E.B. Kruglova, O.P. Pashchuk, Talanta 53 (2000) 233–246.
[38] D.X. Yang, A. Velamakanni, G. Bozoklu, S. Park, M. Stoller, R.D. Piner, S. Stankovich, I. Jung, D.A. Field, C.A. Ventrice Jr., R.S. Ruoff, Carbon 47 (2009) 145–152.
[39] R.J. Tseng, C. Tsai, L.P. Ma, J. Ouyang, C.S. Ozkan, Y. Yang, Nat. Nanotechnol. 1 (2006) 72–77.

[40] J. Liu, T. Qian, M.F. Wang, X.J. Liu, N. Xu, Y.Z. You, C.L. Yan, Nano Lett. 17 (2017) 5064–5070.
[41] F.Y. Fan, W.C. Carter, Y.M. Chiang, Adv. Mater. 27 (2015) 5203–5209.
[42] L. Qie, A. Manthiram, Adv. Mater. 27 (2015) 1694–1700.
[43] J.Q. Zhou, T. Qian, N. Xu, M.F. Wang, X.Y. Ni, X.J. Liu, X.W. Shen, C.L. Yan, Adv. Mater. 29 (2017) 1701294.
[44] X.H. Liu, W.P. Si, J. Zhang, X.L. Sun, J.W. Deng, S. Baunack, St. Oswald, L.F. Liu, C.L. Yan, O.G. Schmidt, Sci. Rep. 4 (2014) 7452.
[45] X. Yang, L. Zhang, F. Zhang, Y. Huang, Y.S. Chen, ACS Nano 8 (2014) 5208–5215.
[46] X.F. Wang, Q.Y. Xiang, B. Liu, L.J. Wang, T. Luo, D. Chen, G.Z. Shen, Sci. Rep. 3 (2013) 2007.
[47] H. Kim, J. Lee, H. Ahn, O. Kim, M.J. Park, Nat. Commun. 6 (2015) 7278.
[48] Z.A. Ghazi, X. He, A.M. Khattak, N.A. Khan, B. Liang, A. Iqbal, J.X. Wang, H. Sin, L.S. Li, Z.Y. Tang, Adv. Mater. 29 (2017) 1606817.
[49] W. Chen, T. Qian, J. Xiong, N. Xu, X.J. Liu, J. Liu, J.Q. Zhou, X.W. Shen, T.Z. Yang, Y. Chen, C.L. Yan, Adv. Mater. 29 (2017) 1605160.
[50] M.U.M. Patel, R. Dominko, ChemSusChem 7 (2014) 2167–2175.